AGU PUBLICATIONS

JGR

Journal of Geophysical Research: Atmospheres

RESEARCH ARTICLE

10.1002/2014JD022944

Key Points:
- Quantification of isotope effects in visible ozone photolysis and $O + O_3$
- Photolysis of ozone in presence of bath gases helium, argon, or carbon monoxide
- Carbon monoxide as $O(^3P)$ quencher to suppress $O(^3P) + O_3$

Supporting Information:
- Table S1
- Tables S2 and S3
- Figure S1
- Figure S2

Correspondence to:
M. Früchtl,
m.fruechtl@uu.nl

Citation:
Früchtl, M., C. Janssen, and T. Röckmann (2015), Experimental study on isotope fractionation effects in visible photolysis of O_3 and in the $O + O_3$ odd oxygen sink reaction, *J. Geophys. Res. Atmos.*, *120*, 4398–4416, doi:10.1002/2014JD022944.

Received 4 DEC 2014
Accepted 8 APR 2015
Accepted article online 16 APR 2015
Published online 14 MAY 2015

Experimental study on isotope fractionation effects in visible photolysis of O_3 and in the $O + O_3$ odd oxygen sink reaction

Marion Früchtl[1], Christof Janssen[2,3], and Thomas Röckmann[1]

[1]Institute for Marine and Atmospheric Research Utrecht, Utrecht University, Utrecht, Netherlands, [2]LERMA, Observatoire de Paris, PSL Research University, CNRS, Paris, France, [3]Sorbonne Universités, UPMC Univ Paris 6, Paris, France

Abstract Investigation of isotope effects in ozone (O_3) photolysis and its contribution to the overall ozone isotope composition is difficult since photolysis always leads to secondary O_3 formation and O_3 decomposition by reactions with $O(^3P)$. Here we use a large excess of carbon monoxide (CO) as $O(^3P)$ quencher to suppress $O(^3P) + O_3$. This allows disentangling the isotope effects in photolysis and chemical removal when the data are evaluated with a kinetic model. The largest systematic uncertainty arises from an unidentified O_3 removal reaction, which is responsible for an unaccounted 20% of the total removal rate. Assuming no isotope fractionation in this reaction, we find ${}^{18}\varepsilon_{O_3+h\nu} = ({}^{16}J/{}^{18}J - 1) = -16.1$ (±1.4)‰ and ${}^{17}\varepsilon_{O_3+h\nu} = -8.05$ (±0.7)‰ for O_3 photolysis and ${}^{18}\varepsilon_{O+O_3} = ({}^{16}k/{}^{18}k - 1) = -11.9$ (±1.4)‰ and ${}^{17}\varepsilon_{O+O_3} = -5.95$ (±0.7)‰ for chemical removal via $O(^3P) + O_3$. Allowing for isotope fractionation in the unidentified reaction results in lower fractionation values for photolysis and higher fractionations for chemical removal. Several fractionation scenarios are examined, which constrain the fractionation in photolysis to ${}^{18}\varepsilon_{O_3+h\nu} > -9.4$‰ and ${}^{17}\varepsilon_{O_3+h\nu} > -4.7$‰ and in the chemical removal to ${}^{18}\varepsilon_{O+O_3} < -18.6$‰ and ${}^{17}\varepsilon_{O+O_3} < -9.3$‰. Both fractionations are thus significant and of similar magnitude. Because our measurements are dominated by photolysis in the peak region of the Chappuis band, isotope fractionation of atmospheric O_3 by visible photons should also be in the same range. The isotope fractionation factor for $O + O_3$ directly bears on ozone chemistry in the lower thermosphere.

1. Introduction

Ozone (O_3) is of great importance for atmospheric chemistry. It is a strong oxidant that contributes significantly to the removal of many carbon-, nitrogen-, and sulfur-containing species in the atmosphere. It is also the precursor of the hydroxyl (OH) radical, which is the principal "cleansing agent" of the atmosphere. Via these two pathways, O_3 determines to a large degree the oxidative capacity of the atmosphere and its ability to absorb harmful UV radiation makes it indispensable to protect life on Earth from radiation emitted from the Sun [*Jacob*, 1999].

In addition, O_3 carries a very peculiar isotopic composition, which can serve as a sensitive marker for chemical reactions involving O_3. Compared to other oxygen containing trace gases, O_3 exhibits very large enrichments in the heavy isotopes of oxygen (^{17}O and ^{18}O) with respect to the oxygen from which it is formed. Isotope enrichments or depletions are reported in the traditional δ notation where $\delta^{18}O = (N({}^{18}O)/N({}^{16}O))_{SA}/(N({}^{18}O)/N({}^{16}O))_{ST} - 1$ quantifies the relative deviation of the ratio $N({}^{18}O)/N({}^{16}O)$ of isotope abundances (indicated by the symbol N) in a sample (SA) from the same ratio in an international standard material (ST). Since deviations are small, δ is usually given in per mill (‰). Contrary to the classical theories of mass dependent isotope effects, the relative enrichments of ^{17}O and ^{18}O show a clear offset from the mass dependent fractionation line. This offset is termed "mass-independent" or "non-mass dependent" fractionation and is quantified in linear form as $\Delta^{17}O \approx \delta^{17}O - 0.52 \times \delta^{18}O$ [*Brenninkmeijer et al.*, 2003].

First evidence for an anomalous isotopic composition of O_3 came from stratospheric balloon measurements, which revealed unexpectedly strong ^{18}O enrichments [*Mauersberger*, 1981]. In the laboratory, *Heidenreich and Thiemens* [1983] produced O_3 by an electric discharge and found that the magnitude of the enrichment was similar for ^{17}O and ^{18}O. These findings triggered many laboratory and atmospheric studies, and the ozone system and its isotope anomaly were investigated thoroughly [*Morton et al.*, 1990; *Mauersberger et al.*, 1993, 1999, 2001; *Anderson et al.*, 1997; *Janssen et al.*, 1999, 2001, 2003; *Johnson et al.*, 2000; *Chakraborty and Bhattacharya*, 2003; *Haverd et al.*, 2005; *Krankowsky et al.*, 2007].

It has soon been established that the process of O_3 formation via the three body reaction $O(^3P) + O_2 + M$ is the driving factor behind the observed anomalies [*Morton et al*., 1990]. Detailed information is available on the dependence of the isotopic fractionation on temperature and pressure of the gas in which O_3 is formed. At pressures above 130 hPa, the enrichment of $^{49}O_3$ (a combination of $^{16}O^{16}O^{17}O$ and $^{16}O^{17}O^{16}O$) and $^{50}O_3$ ($^{16}O^{16}O^{18}O$ and $^{16}O^{18}O^{16}O$) decreases and almost disappears at pressures near 20 atm. Furthermore, isotope enrichments decrease with decreasing temperatures. At 300 K, the enrichment of $^{50}O_3$ is higher compared to $^{49}O_3$, but below 200 K the enrichments undergo a crossover [*Morton et al*., 1990]. The systematic variation of the enrichment for certain isotopomers suggests that molecular symmetry effects might play an important role in the isotope effect found in the O_3 formation reaction [*Mauersberger et al*., 1993; *Anderson et al*., 1997; *Gao and Marcus*, 2001].

A major breakthrough in the understanding of the O_3 isotope effect came with detailed studies of individual isotope specific rate coefficients. It was shown that collisions between light atoms (^{16}O) and heavy molecules ($^{17}O^{17}O$ and $^{18}O^{18}O$) have a rate coefficient advantage of about 25 and 50% relative to the formation reaction involving ^{16}O and $^{16}O^{16}O$ [*Anderson et al*., 1997; *Mauersberger et al*., 1999]. O_3 formation from heavy atoms and light molecules, on the other hand, is relatively slow.

Experimental results on the relative temperature dependence of individual rate coefficients showed no temperature dependence for O_3 formation channels with high relative rate coefficients (e.g., $^{16}O + {}^{18}O^{18}O$), while the rate coefficients for slow formation channels such as $^{18}O + {}^{16}O^{16}O$ decreased with decreasing temperatures [*Janssen et al*., 2003]. In subsequent studies, rate coefficients for many possible isotopic combinations of reactants O and O_2 were measured [*Anderson et al*., 1997; *Janssen et al*., 1999, 2001].

A number of attempts have been made to unravel the molecular processes behind the isotopic anomaly in O_3. The mass-independent isotope enrichment observed in the laboratory could be reproduced well in the framework of RRKM (Rice-Ramsperger-Kassel-Marcus) theory when an empirical nonstatistical factor η (non-RRKM effect) was applied to describe the difference in the density of active metastable states (O_3*) in symmetric and nonsymmetric O_3 molecules. Differences in zero point energies of the two transition states in O_3 formation were identified as the dominant factor controlling the lifetime of the O_3* and, therefore, causing the differences in the relative rate coefficients [*Gao and Marcus*, 2002]. Quantum mechanical calculations showed a strong nonstatistical feature of the lifetime of the metastable O_3*. The number of ozone metastable states decays through three different $O_2 + O$ channels. Many metastable states occur at energies below the zero point energy thresholds, while only few occurred above it. The low-lying metastable states could be stabilized faster since they have a longer lifetime. The differences in the lifetime spectrum result from differences in zero point energy of the two formation channels $^{16}O + {}^{18}O^{18}O \rightarrow {}^{16}O^{18}O^{18}O$ and $^{16}O^{18}O + {}^{18}O \rightarrow {}^{16}O^{18}O^{18}O$ [*Babikov et al*., 2003].

Comparison of laboratory results with early vertical profile measurements in the atmosphere between 22 and 40 km using mass spectrometry [*Mauersberger et al*., 2001] as well as balloon-based far infrared thermal emission solar occultation spectra [*Johnson et al*., 2000] supported the hypothesis that the isotopic anomaly in O_3 originates from the O_3 formation reaction only. However, later stratospheric measurements demonstrated that temperature effects in O_3 formation could explain the enrichments of the heavy isotopologues $^{49}O_3$ and $^{50}O_3$, up to 27 km only. Above that altitude, the enrichments rose faster than expected from the temperature effect only [*Krankowsky et al*., 2007]. Very large enrichments have been reported at higher altitudes based on balloon-borne remote sensing [*Haverd et al*., 2005]. It was suggested that a fractionation in the removal of O_3, in particular UV photolysis, could have an additional effect on its isotopic composition.

Chakraborty and Bhattacharya [2003] showed in an experimental setting different fractionation patterns for ozone photolyzed with UV (184.9 and 253.6 nm) or visible light (520 and 630 nm). Dissociation in the Chappuis band showed a mass dependent character with a three-isotope slope $\delta^{17}O/\delta^{18}O$ of 0.54, whereas dissociation in the Hartley band was mass-independent (slope 0.63). However, a later modeling study by *Cole and Boering* [2006] attributed the mass-independent effect reported by Chakraborty and Bhattacharya to formation of new O_3 during the UV photolysis experiments.

Nevertheless, analysis of experimental absorption spectra by *Miller et al*. [2005] suggested that O_3 photolysis is associated with a wavelength-dependent fractionation with large variations in the fractionation constants over few nanometers. Photolytic modeling results attributed up to +45‰ of the O_3 anomaly in the middle

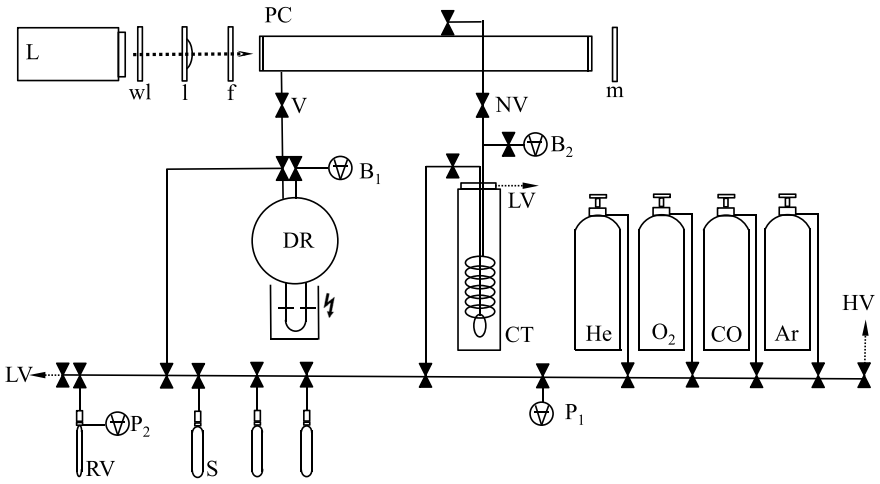

Figure 1. Gas handling and O_3 photolysis system. Definition of abbreviations: Discharge reactor (DR), photolytic chamber (PC), lamp (L), water lens (wl), lens (l), filter (f), mirror (m), cryogenic trap (CT), sample bottle (S), reference volume (RV), low-vacuum membrane pump (LV), high-vacuum pump (HV), valve (V), needle valve (NV), P_1 P_2 (pressure sensors), and B_1 B_2 (Baratron pressure sensors).

stratosphere to ozone photolysis effects [*Miller et al.*, 2005]. Additionally, the vertical profiles between 15 and 40 km altitude of *Haverd et al.* [2005] showed fractionations for $^{16}O^{16}O^{18}O$ and $^{16}O^{18}O^{16}O$ that were in good agreement with already published data of 13.5 ± 2.7% and 7.7 ± 2.2%, respectively, for an average of 20–35 km. However, the fractionations showed a clear increase with altitude of 3.5 ± 2.2% and 4.0 ± 1.6% for $^{16}O^{16}O^{18}O$ and $^{16}O^{18}O^{16}O$ over the 20–35 km range, and therefore deviated from those expected from temperature effects only. Also a modeling study by *Liang et al.* [2006] in which the altitude variation of heavy O_3 is combined with the known formation-induced isotope effects, enrichments were systematically higher than the observations by 1 to 1.5%.

Investigation of the role of O_3 photolysis and its contribution to the O_3 isotope effect is difficult [*Brenninkmeijer et al.*, 2003], because photolysis inevitably leads to the following reactions:

$$O_3 + h\nu \rightarrow O(^3P) + O_2 \quad \text{(R1)}$$

$$O(^3P) + O_2 + M \rightarrow O_3 + M \quad \text{(R2)}$$

$$O(^3P) + O_3 \rightarrow 2O_2 \quad \text{(R3)}$$

This implies that the photolysis reaction (R1) cannot easily be separated from secondary O_3 formation (R2) or the O_3 decomposition in reaction with $O(^3P)$ (R3). In particular, in laboratory photolysis experiments with pure O_3 samples, (R1) will always occur simultaneously with reaction (R3), so that the observed fractionation is the average of these two removal channels. In addition, when O_2 builds up in the reactor as the experiment proceeds, (R2) will become progressively more important.

In this study, we attempt to disentangle the isotope effects in the different reactions by using carbon monoxide (CO) as $O(^3P)$ quencher:

$$O(^3P) + CO + M \rightarrow CO_2 + M \quad \text{(R4)}$$

When using a large excess of CO, it is possible to strongly suppress reactions (R2) and (R3). To exclude isotope effects related to excited electronic states of oxygen, we investigate the fractionation effect in visible photolysis (455–800 nm) of O_3. Results are interpreted using a kinetic model.

2. Methods

2.1. System Description

The gas handling and O_3 photolysis system is mostly made out of Pyrex glass (Figure 1). Valves are either glass with Teflon O-rings (Glass Expansion, Australia) or Teflon only valves (Young, England). Metal parts are

avoided wherever possible and remaining metal surfaces, which connect to pressure sensors (Baratron, MKS, range 10 and 100 Torr: Scientific Solutions Ltd., Institute of Geological and Nuclear Sciences Limited), the high-vacuum turbo pump (HighCube, Pfeiffer, 1500 Hz), the low-vacuum membrane pump with end pressure of 10^{-3} hPa (KNF Neuberger), and the gas supplies can be separated from the system with additional Teflon-sealed valves. The material of the gas lines is stainless steel for He, Ar, and O_2. CO is injected through a copper line. The base vacuum achieved by the system is ~ 10^{-6} hPa (measured at the pump).

The setup for the photolysis experiments consists of three major parts. A ~1.0 L discharge reactor where O_3 is created from electric discharge in pure oxygen, a photolysis chamber in which O_3 is photolyzed, and a cold trap which serves to collect O_3.

The spherical 12 cm diameter discharge reactor (Schott Duran®) has a 12.5 cm long and 3 cm wide cylindrical extension, which can be immersed in liquid nitrogen. It contains two electrodes that are attached to a 1500V AC power supply. Two glass coated tungsten wires enter the reactor finger from two opposite sides and are installed at a distance of 1 cm inside the reactor volume. For fast O_3 production, the electrodes can be fully immersed in liquid nitrogen. O_3 is removed from the gas phase by condensation on the reactor walls. At the upper part, two valves separate the discharge reactor from the glass line and the photolysis chamber. Additionally, in order to determine the pressure, a high-accuracy pressure sensor is attached at the top of the reactor.

The cylindrical photolysis chamber ($V = 630$ cm^3, $l = 50$ cm, and $d = 4$ cm) is placed horizontally behind the discharge reactor. The reactor walls are made out of silica glass. The quartz glass (Suprasil) windows are highly transparent from the UV to the IR wavelength region and glued to both ends of the reactor using epoxy glue (Scotch-Weld™, DP 100, 3M). The reactor is externally shielded with aluminum foil. The gas inlet of the photolysis chamber is directly connected to the discharge reactor. The gas outlet is connected to the O_3 collection trap. For precise gas handling, a Teflon needle valve is placed between these two components.

At a distance of 22 cm from the photolysis chamber, a halogen photo optic Xenophot® lamp ($U = 15.9$ V, $I = 10.58$ A, type HLX 64633) equipped with an elliptic mirror is used as light source. The spectral distribution of the lamp has been calibrated using a spectral photometer. The lamp shows a broad emission peak centered at 605 nm. However, it also emits some UV radiation, which contributes significantly to O_3 photolysis due to the high-absorption cross section of O_3 in the Hartley band (see supporting information Figure S1). We prevent UV photolysis by placing an optical filter cutting off radiation with wavelengths shorter than 455 nm directly in front of the photolysis chamber.

In order to filter out IR radiation and, therefore, to reduce temperature effects, a 77 cm^3 water lens that is constantly flushed with distilled water, is installed between the lamp and the photolysis chamber. An aspherical condenser lens with effective focal length of 18 mm (Edmund Optics) and a diameter of 5 cm is placed at a distance of 16 cm from the lamp to focus the light into a parallel beam. A flat surface mirror with enhanced aluminum coating (reflection $>$95%) is added at the end of the photolysis chamber in order to reflect back photons into the chamber and thus to increase the photolysis rate.

After photolysis, the remaining ozone is collected in a cryogenic trap, which is connected to a vacuum pump and cooled to 63 K by pumping on the vapor when placed in liquid nitrogen. The O_3 trap contains two additional valves, which are used to separate the trap from the rest of the glass line.

For isotopic analysis, O_3 or O_2 is collected in a 44.2 cm^3 sample bottle containing approximately 10 pellets of molecular sieve (13X 1.6 mm pellets, Sigma Aldrich) dipped in liquid nitrogen.

The 1.8 cm^3 reference volume used to quantify the amount of gas after an experiment has a pressure sensor attached and contains either molecular sieve (13X 1.6 mm pellets, Sigma Aldrich) or high purity nickel (Ni) foil (annealed, thickness 0.05 mm, 99.98% purity, Goodfellow, Cambridge Ltd.)

Isotopic ratios are measured using a Delta^{Plus}XL (Thermo Finnigan) mass spectrometer. Typical internal uncertainties are 0.03‰ in $\delta^{18}O$ and 0.08‰ in $\delta^{17}O$ (standard deviation of 10 sequences, 15 runs each, $n = 150$).

For the experiments, we use helium (He) of 99.9997% purity (Air products) and ultra pure plus oxygen (O_2) of 99.9998% purity (Air products) with isotopic composition of $\delta^{17}O = 9.5$ (±0.03)‰ and $\delta^{18}O = 18.9$ (±0.05)‰

versus Vienna standard mean ocean water (VSMOW). The CO used has a purity of 99.997% (Linde) and its isotopic composition is $\delta^{13}C = -54.4$ (±0.2)‰ versus Vienna Peedee belemnite and $\delta^{18}O = -6.0$ (±0.3)‰ versus VSMOW.

2.2. Experimental Procedure

Three sets of experiments were carried out to investigate the role of O_3 dissociation processes, in particular photolysis and the $O_3 + O$ reaction, in detail. In set 1, O_3 only was photolyzed for different time periods (named O_3 *only*). In sets 2 and 3, O_3 was either mixed with He (O_3 + He), Ar (O_3 + Ar), or CO (O_3 + CO) bath gas before photolysis of the mixture. To test the efficiency of the extraction system and the stability of O_3 in the analytical system, runs without photolysis were carried out for the above three sets of experiments (i.e., the same procedure was applied but without turning on the photolysis lamp).

For each set of experiments, O_3 was generated from 8.5 hPa pure O_2 in the discharge reactor. After filling the reactor with O_2, the cylindrical extension, including the electrodes, was immersed in liquid nitrogen. The electric discharge was turned on for about 1 min during which liquid O_3 condenses on the reactor walls. After the discharge was switched off at ~ 6 hPa, the remaining O_2 was pumped away until a residual pressure of 5 Pa was reached. Thereafter, the liquid nitrogen was removed and the condensed O_3 was brought to the gas phase at room temperature. After complete evaporation of O_3, different bath gases, depending on the experiment, were admitted to the discharge reactor. Gases were mixed in ratios of ~ 1: 900 (O_3 : bath gas).

The gas mixture was transferred into the photolysis chamber by opening and closing the valve between discharge reactor and photolysis chamber. In the following, we call this step *expansion*. In order to assure complete mixing in the discharge reactor and its connections to the valves, a first fraction of the gas mixture was expanded into the photolysis chamber for conditioning it and then pumped away. Only the second and third expansions into the photolysis chamber were used for experiments. Standing times of the gas mixture in the discharge reactor varied between 45 min (second expansion) and 4 h (third expansion), depending on the type of experiment. Evacuation times for experiments with CO were longer than those with He or O_3 only.

Irradiation times were varied between 5 and 30 min. For comparison of O_3 before and after photolysis, the second expansion was used for photolysis while the third expansion was sampled without photolysis in order to determine the isotopic composition of the starting O_3. This was necessary since the isotopic composition of O_3 generated by electric discharge showed small differences of 1 and 2‰ in $\delta^{17}O$ and $\delta^{18}O$, respectively, depending on small variations in discharge time.

After photolysis, the remaining O_3 was collected in the cryogenic trap at 63 K. When all O_3 was collected, the trap was isolated and the liquid nitrogen was removed. O_3 was brought to room temperature by warming the trap with a small beaker filled with room temperature water.

O_3 was then transferred to a sample bottle cooled down to liquid nitrogen temperature and containing approximately 10 pellets of molecular sieve. Additional heating of the sample led to complete conversion of the O_3 sample into O_2. The O_2 was then cryogenically transferred to the reference volume using molecular sieve at liquid nitrogen temperatures. To determine the amount of molecular oxygen, the liquid nitrogen was removed and the sample bottle was warmed with room temperature water and the pressure was taken. Thereafter, the sample was frozen back at liquid nitrogen temperature on molecular sieve in the original sample bottle. As mentioned above, immediately after recovering the O_3 from the photolysis experiment, another aliquot was expanded from the discharge reactor into the photolysis reactor in order to determine the amount and isotopic composition of the starting O_3. CO_2 produced from the O + CO reaction or potentially other sources remained in the molecular sieve and, therefore, could not interfere with the O_2 isotopic analysis.

An additional set of experiments was performed in order to evaluate the trapping and purification procedure. In these experiments, O_3 and CO_2 from reaction (R4) were directly transferred to the reference volume using liquid nitrogen. After warming the reference volume, which contained small strips of Ni-foil, in a water bath at room temperature, the $O_3 + CO_2$ pressure was measured. Subsequent heating for 3 min at 80°C led to catalytic conversion of O_3 to O_2. Thereafter, the reference volume was brought to room temperature again and the $O_2 + CO_2$ pressure was recorded. In a last step, the reference volume was immersed in liquid nitrogen to trap

CO_2, while the molecular oxygen was transferred to a sample bottle filled with molecular sieve and held at liquid nitrogen temperature. After the CO_2 pressure was determined by warming up the reference volume, the sample was cryogenically transferred to a sample bottle. Since 1.5 moles of O_2 are formed from decomposition of one mole of O_3, the O_3 pressure in the reference volume was calculated from the two pressure measurements ($O_3 + CO_2$ and $O_2 + CO_2$) according to

$$p_{O_3} = 2\times\left[p_{(O_2+CO_2)} - p_{(O_3+CO_2)}\right]. \quad (1)$$

The sample bottle containing pure O_2 derived from O_3 was then attached to the sample inlet of the dual inlet isotope ratio mass spectrometry and measured relative to our O_2 laboratory standard.

In the following, we refer to the O_3 sample measured after photolytic destruction as O_3(*end*). The extraction from the expansion carried out directly after the photolysis experiment and without irradiation of the gas mixture is representative for the original O_3 produced in the electric discharge and is referred to as O_3 (*start*). The ratio O_3(end)/O_3(start) (corrected for an additional volume expansion of O_3(start)) defines the remaining fraction $f(O_3)$, which quantifies the O_3 conversion for a certain photolysis period:

$$f(O_3) = O_3(\text{end})/O_3(\text{start}). \quad (2)$$

2.3. Model Details

2.3.1. Reaction Scheme

The reaction kinetics of the gas mixture exposed to visible light only (by using a 455 nm band-pass filter) was simulated using the chemical kinetics software Kintecus® [*Ianni*, 2003]. Three sets of model runs were employed to simulate the three sets of experiments: (a) O_3 only photolysis, (b) photolysis in the presence of He or Ar, and (c) photolysis in the presence of CO. The model allows to quantitatively interpreting the experiments, because the different reaction pathways of O atoms in the different experiments can be quantified.

Four chemical reactions (R1)–(R4) and two isotope exchange reactions (R5a), (R5b), and (R6) were included in our photochemical model.

$$O_3 + h\nu \rightarrow O(^3P) + O_2, \qquad J_{O_3} = 3.4\times10^{-4}s^{-1} \quad (R1)$$

$$O(^3P) + O_2 + M \rightarrow O_3 + M, \qquad k_2 = 6.0\times10^{-34}(300K/T)^{-2.4}cm^6s^{-1} \quad (R2)$$

$$O(^3P) + O_3 \rightarrow O_2 + O_2, \qquad k_3 = 8.0\times10^{-12}\exp(-2060K/T)cm^3s^{-1} \quad (R3)$$

$$O(^3P) + CO + M \rightarrow CO_2 + M, \qquad k_4 = 2.56\times10^{-36}cm^6s^{-1}(T = 306K,\ p = 613hPa) \quad (R4)$$

$$Q + OO \leftrightarrow QO + O, \qquad k_{5a} = 3.4\times10^{-12}(300K/T)^{1.1}cm^3s^{-1} \quad (R5a)$$

$$O + QQ \leftrightarrow OQ + Q, \qquad k_{5b} = 2.7\times10^{-12}(300\ K/T)^{0.9}cm^3s^{-1}) \quad (R5b)$$

$$O + CO \leftrightarrow CO + O, \qquad k_6 = 1.65\times10^{-11}\exp(-2730K/T)\ cm^3s^{-1} \quad (R6)$$

The rate coefficient applied for O_3 photolysis (R1) was determined experimentally as explained in detail in section 3.1. Rate coefficient values (R2) and (R3) are given based on recent recommendations [*Sander et al.*, 2011]. Values for k_{5a} and k_{5b} are adopted as given in *Fleurat-Lessard et al.* [2003]. For isotopic exchange of O and CO, rate coefficient k_6 is based on *Jaffe and Klein* [1966]. The value of k_4 is derived from studies by *Slanger et al.* [1972], *Simonaitis and Heicklen* [1972], and *DeMore* [1972] in section 2.3.3, where the bath gas dependence of k_2 is also discussed.

Most important for the interpretation of the results is the fate of O atoms produced in (R1). They can either react with another O_3 molecule (R3), be quenched away by CO (R4) or form new O_3 (R2), with relative importance of these pathways depending on experimental conditions.

The model results shown in Figure 2 confirm that during photolysis of pure O_3 with visible light, virtually all of the O atoms produced within the first 30 min destroy another O_3 molecule via (R3) ($O + O_3$). Formation of new O_3 becomes significant only after 30 min. In sharp contrast, the presence of He bath gas strongly increases the formation process, and both pathways ($O + O_3$ and O_3 formation via $O + O_2 + M$) contribute approximately equally after 25–30 min. When CO is used as bath gas, the reaction $O + CO$ quenches away about 75–80% of the O atoms and the reaction $O + O_3$ is strongly suppressed, which was intended by this study. Nevertheless, even at a mixing ratio of 1:900 (O_3/CO), $O + O_3$ still consumes about 25% of

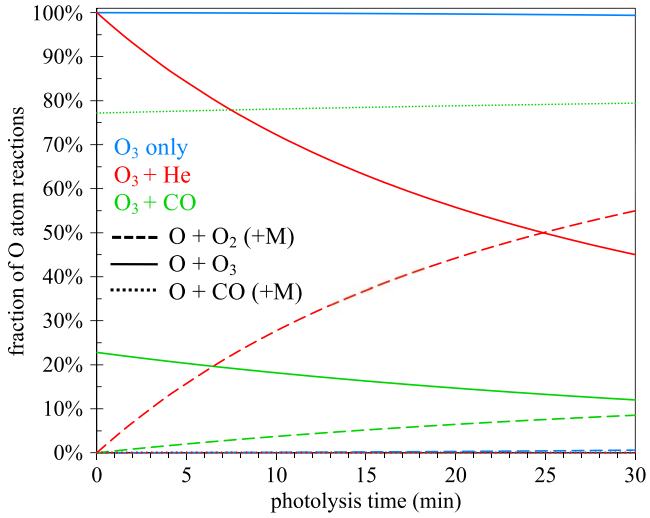

Figure 2. Fractions of O atoms lost via the three different reaction channels in percent. Long-dashed lines: $O + O_2$ (+M). Solid lines: $O + O_3$. Short-dashed lines: O + CO (+M). The three types of experiments are shown in different colors. Blue: O_3 only; red: O_3 in He bath gas; and green: O_3 in CO bath gas.

the O atoms at the start. O_3 formation is actually increased compared to the O_3 only case, because CO also serves as a third body reaction partner (M) in (R4), thus increasing the rate of ozone formation.

2.3.2. Isotopes

Isotopic enrichments are calculated from modeled molecular abundances. The model explicitly calculates all possible isotopic combinations of all the above six reactions using the following labeling P = ^{17}O, Q = ^{18}O, and O = ^{16}O. It also includes known or assumed isotope effects for the variants of reactions (R1)–(R6). This increases the number of reactions to 159 (Table 1).

The model input for initial concentrations of O_3 ($^{16}O_3$) and bath gases corresponds to the experimental conditions. Initial O_3 number densities are 2.87×10^{16}, 1.52×10^{16}, 1.61×10^{16}, and $1.67\times10^{16}\,cm^{-3}$ for the O_3 only, the He, Ar, and the CO experiments, respectively. Bath gas number densities are 1.34×10^{19} (547 hPa; He/O_3 = 886.5), 1.49×10^{19} (607 hPa; Ar/O_3 = 925.3), and $1.45\times10^{19}\,cm^{-3}$ (591 hPa; CO/O_3 = 868.5) for the He, Ar, and CO runs. All initial concentrations represent an average of the photolysis experiments of each data set.

For illustration purposes, we derive in the following the number density of asymmetric (OOQ) and symmetric (OQO) $^{50}O_3$, assuming a statistical distribution of isotopes. The molecule specific abundance is calculated from the atomic abundance ratio, $^{18}R_{O_3} = (N(Q)/(O))_{O_3}$ where N(O) and N(Q) stand for the absolute number of receptive O and Q atoms of ozone in a given volume, and one obtains

$$\frac{[OOQ]}{[OOO]} = 2\times\left(^{18}R_{O_3}\right) \qquad \frac{[OQO]}{[OOO]} = {}^{18}R_{O_3}. \tag{3}$$

Therefore the initial number density of OOQ is calculated as follows:

$$[OOQ]_{initial} = [OOO]_{initial}\times 2(^{18}R_{O_3}), \tag{4}$$

and initial [OQO] is correspondingly given by

$$[OQO]_{initial} = [OOO]_{initial}\times {}^{18}R_{O_3}. \tag{5}$$

Isotope specific enrichments are calculated from modeled molecular abundances. The definition of $\delta^{18}O$ is based on the atomic abundance ratio

$$\delta^{18}O = \frac{\left(\frac{N(^{18}O)}{N(^{16}O)}\right)_{SA}}{\left(\frac{N(^{18}O)}{N(^{16}O)}\right)_{ST}} - 1 \tag{6}$$

in the sample (SA) and the standard (ST), implying that all relevant species containing a heavy oxygen need to be summed up and divided by the number of species containing a light oxygen (^{16}O). For O_2, we obtain

$$^{18}R_{O_2} = \frac{2[Q_2] + [OQ] + [QP]}{2[O_2] + [OQ] + [OP]}. \tag{7}$$

Table 1. List of Main Reactions in Kinetic Model[a]

Reaction	Number of Variants	Reaction Type
(R1)	27	$O_3 + h\nu \rightarrow O + O_2$
(R2)	27	$O + O_2 + M \rightarrow O_3 + M$
(R3)	72	$O + O_3 \rightarrow O_2 + O_2$
(R4)	9	$O + CO + M \rightarrow CO_2 + M$
(R5a) and (R5b)	18	$Q + OO \leftrightarrow QO + O$
(R6)	6	$Q + CO \leftrightarrow CQ + O$
(R7)	(81)	$(O_3 + CO \rightarrow CO_2 + O_2)$

[a]Included are reactions with multiple substitutions. Number of variants for (R2) increase to 270 under consideration of O_3 = M.

Calculation of ${}^{18}R_{O_3}$ involves 18 species, if the intramolecular isotope distribution is taken into account. This leads to

$$ {}^{18}R_{O_3} = \frac{[OOQ] + [OQO] + 2[OQ_2] + 2[QOQ] + [POQ] + [OPQ] + [OQP] + 2[PQ_2] + 2[QPQ] + [PPQ] + [PQP] + 3[Q_3]}{3[O_3] + 2[O_2Q] + 2[OQO] + 2[OOP] + 2[OPO] + [OPP] + [POP] + [OQ_2] + [QOQ] + [POQ] + [OPQ] + [OQP]}. \quad (8) $$

Note that similar formulas apply to the definition of $\delta^{17}O$ and to other oxygen containing molecules. For calculating ${}^{18}R_{O_3}$, our model considers all possible isotopic substitutions, while in mass spectrometric analysis, species containing two or three heavy oxygen atoms are excluded. However, model runs excluding double and triple substituted species only differ in a magnitude of 0.1‰ for ^{18}O and 0.06‰ for ^{17}O from model runs including all isotopic substitutions.

2.3.3. Rate Coefficients

The O_3 photolysis rate coefficient has been determined experimentally (see section 3.1.). O_3 formation rates are based on the currently recommended value for air [*Sander et al*., 2011] using the relative third body efficiencies of 1, 0.6, 0.74, 1.06, and 2.27 for O_2, He, Ar, CO, and O_3, respectively. Values for O_2, He, and O_3 were taken from the recommendation of *Steinfeld et al*. [1987], while the factor used for Ar originates from a relatively recent study of *Hippler et al*. [1990]. This study has been performed at higher pressures than most of the previous work. Except for Ar, values agree very well with the older recommendation of *Steinfeld et al*. [1987] as far as the bath gas dependency is concerned. The CO efficiency is the average of two pulsed radiolysis studies performed by *Maeburn et al*. [1968] and by *Stuhl and Niki* [1971], which are the only experiments in CO that we are aware of.

The reaction coefficient for CO + O (R4) is not very well constrained by previous studies. After a thorough literature survey, we use low- and high-pressure limiting rates of $k_0 = 6.5 \times 10^{-33}\ \exp(-2184\ \mathrm{K/T})\ \mathrm{cm^6\ s^{-1}}$ and $k_\infty = 2.66 \times 10^{-14}\ \exp(-1460\ \mathrm{K/T})\ \mathrm{cm^3\ s^{-1}}$, respectively. The low-pressure limiting value k_0 corresponds to the results of *Slanger et al*. [1972], which are considered to be free of contamination effects that have affected many of the earlier studies [*Baulch et al*., 1976]. The pressure dependence of the reaction is complex and cannot simply be described using a single falloff region, and the above value of k_∞ fails to describe the high-pressure behavior [*DeMore*, 1972]. Similarly, the rate of the O + CO isotope exchange determined by *Jaffe and Klein* [1966] does not correspond to the high-pressure limiting rate coefficient that would reproduce a falloff already at about 1 atmosphere, as observed by *Simonaitis and Heicklen* [1972] and *DeMore* [1972]. Only at much higher pressures, a second falloff consistent with the results of *Jaffe and Klein* [1966] is observed [*DeMore*, 1972]. Being concerned with pressures at and below 1 atm only, we nevertheless adopt the value $k_\infty = 2.66 \times 10^{-14}\ \exp(-1460\ \mathrm{K}/T)\ \mathrm{cm^3\ s^{-1}}$ of *Simonaitis and Heicklen* [1972], which is suited to reproduce the pressure dependence in that range. The value is based on measurements at pressures of slightly above 1 atm of CO mixed with nitrous oxide (N_2O) and corresponds to a second-order rate coefficient of $2.04 \times 10^{-16}\ \mathrm{cm^3\ s^{-1}}$ at 300 K. *DeMore* [1972] finds a similar value of $k_\infty = 1.9 \times 10^{-16}\ \mathrm{cm^3\ s^{-1}}$ for the pressure range below 2 atm, above which the pseudo second-order rate becomes pressure dependent again. The latter value, which agrees very well with the result of *Simonaitis and Heicklen* [1972] takes into account a scaling to the actually recommended rate coefficient for the $O + O_2 + M$ reaction using relative quenching efficiencies of 1/2.7 for $(N_2)/CO_2$, because these experiments have relied on O_3 formation in CO_2 and N_2, as a reference to determine O atom abundances.

Using the standard expression for the rate coefficient in the falloff region [*Sander et al*., 2011],

$$ k_f([M]) = \frac{k_0}{[M]^{-1} + \frac{k_0}{k_\infty}} 0.6^{\left\{1 + \left[\log_{10}\left(\frac{k_0[M]}{k_\infty}\right)\right]^2\right\}^{-1}}, \quad (9) $$

the rate coefficient of (R4) is obtained from k_0 and k_∞. Under our conditions, at 306 K and 613 hPa of CO, we find the value of $k_4 = 3.71 \times 10^{-17}\ \mathrm{cm^3\ s^{-1}}$, or $k_4/[M] = 2.56 \times 10^{-36}\ \mathrm{cm^6\ s^{-1}}$, when expressed as termolecular rate coefficient.

Rates for the isotopic exchange of O with O_2 and CO are based on available rate coefficient data [*Jaffe and Klein*, 1966; *Fleurat-Lessard et al*., 2003] and isotope exchange equilibrium constants. For a detailed list, see supporting information Tables S1 and S2.

2.3.4. Fractionation Coefficients

Fractionation coefficients for O_3 formation (R2) are directly adopted from *Janssen et al.* [1999] and *Mauersberger et al.* [1999] or are derived from empirical zero point energy relationship described in *Mauersberger et al.* [2002] and *Babikov et al.* [2003]. To include the pressure dependence of the O_3 formation kinetic isotope effects, we apply calculations from *Wiegel et al.* [2013]. In their study, the pressure dependent isotope effect is derived from the O_3 formation kinetic isotope effect at low pressure and the pressure dependence of the O_3 isotopic enrichments.

For CO_2 formation, no fractionation coefficients are applied, since up to now, no values for this reaction are given in published literature.

For isotopic exchange $O + O_2$, we use fractionation factors based on calculations by *Janssen and Tuzson* [2010]. Adopted values are 2.1563 and 2.0810 for the ^{18}O and ^{17}O isotope exchange at 306 K.

The calculation we used to determine fractionation factors for the isotopic exchange $O + CO$ is based on the classical Urey approach [*Urey*, 1947; *Richet et al.*, 1977] and neglects nuclear spin effects in the case of ^{17}O and the fact that molecular oxygen in its ground electronic $^3\Sigma$ state is an open shell molecule, which gives rise to a fine structure beyond the coupled linear rotor-harmonic oscillator approximation. Nevertheless, the result at 300 K is reasonable close (3‰ for ^{18}O) to the results of calculations based on molecular spectroscopic data [*Fischer et al.*, 2003; *Rothman et al.*, 2013]. Since CO is a closed shell molecule, the Urey approach is directly applicable and we have obtained values of 1.1027 and 1.0530 for $^{18}O + CO$ and $^{17}O + CO$, respectively. This is in full agreement with the tabulated results of *Richet et al.* [1977].

We derive isotopic fractionation coefficients for O_3 photolysis (R1) and O_3 decomposition (R3) by fitting the model results to the measurements. The O_3 only experiments allow deriving the combined fractionation values for O_3 photolysis and O_3 destruction via $O + O_3$.

$$\varepsilon_{O_3\text{only}} = (\varepsilon_{O_3+h\nu} + \varepsilon_{O_3+O})/2. \tag{10}$$

By using CO as an O atom quencher, reaction $O + O_3$ is suppressed and we can separate fractionation processes in both channels, $O_3 + h\nu$ and $O_3 + O$. Including O_3 formation $\left(\varepsilon_{O_2+O+M} \times g_{O_2+O+M}\right)$, the combination of different fractionation processes gives

$$\varepsilon_{O_3+CO} = \left(\varepsilon_{O_3+h\nu} \times g_{O_3+h\nu} + \varepsilon_{O_3+O} + g_{O_3+O} + \varepsilon_{O_2+O+M} \times g_{O_2+O+M}\right), \tag{11}$$

where weights g denote the relative contributions of each channel to the overall ε_{O_3+CO}.

3. Results

3.1. Photolysis Rate

The photolysis rate is the key quantity that rules the speed of the experiment, and it is determined in two independent ways. First, it is derived from the pressure increase in the reaction vessel during a typical O_3 photolysis experiment. The sum of reactions (R1) and (R3) is 2 O_3 ➔ 3 O_2, which leads to the isothermal increase of pressure (p) during photolysis:

$$J_{O_3} = -\frac{1}{2[O_3]} \times \frac{d[O_3]}{dt} = \frac{1}{p} \times \frac{dp}{dt} \tag{12}$$

Note that the relative change of the O_3 number density in (12) has been divided by a factor of 2 (since only one half of the O_3 molecules are actually destroyed by photolysis, the other half by $O + O_3$). In practice, the observed increase in pressure during photolysis needs to be corrected for temperature effects, which were obtained from a similar experiment with pure O_2. The photolysis rate obtained in this way is $J_{O_3} = 3.2\ (\pm 0.1) \times 10^{-4}\ s^{-1}$, which is an average of four measurements with a photolysis time of 30 min each. J_{O_3} can also be determined directly from the loss of O_3 as a function of photolysis time as

$$J_{O_3} = 0.5\ \ln(f)/t, \tag{13}$$

where f is the above defined remaining O_3 fraction after t seconds of photolysis. This approach yields $J_{O_3} = 3.4 \times 10^{-4}\ s^{-1}$, which is in good agreement with the result from the pressure measurements. Since the

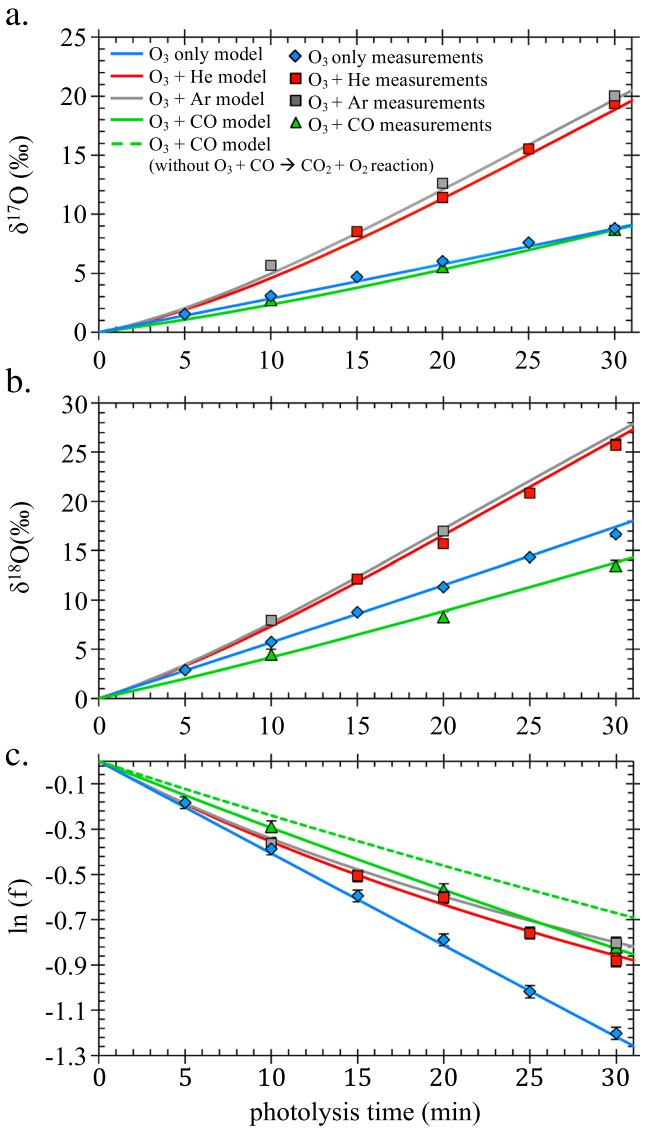

Figure 3. Temporal evolution of (a) $\delta^{17}O$ and (b) $\delta^{18}O$ and (c) remaining fraction ln(f) of O_3 during a photolysis experiment**.** Experiments in various bath gases are shown with different colors. Blue: pure O_3, red: He bath gas, grey: Ar bath gas, and green: CO bath gas. Filled symbols represent measurements; solid lines represent model runs. Fractionations applied in the modeling are $\varepsilon_{O_3+h\nu} = -16.1$ and -8.05‰ for ^{18}O and ^{17}O; for $\varepsilon_{O_3+O} = -11.9$‰ and -5.95‰ for ^{18}O and ^{17}O, respectively. Model runs include the additional O_3 removal reaction $O_3 + CO$ that is relevant in presence of CO. No fractionations are applied for the $O_3 + CO$ reaction. The dashed green line represents the O_3 removal in CO bath gas, without consideration of an additional O_3 removal reaction. Error bars are 1σ.

latter value is directly derived from the photolysis experiments, we use this photolysis rate in the model; the assigned uncertainty is $0.2 \times 10^{-4}\,s^{-1}$.

Some experiments that were performed at a later time showed changes in the photolysis rate due to lamp aging. The photolysis rate decreased to a value of $J_{O_3} = 2.9 \times 10^{-4}\,s^{-1}$. The experimental results obtained with $J_{O_3} = 2.9 \times 10^{-4}\,s^{-1}$ have been scaled to $J_{O_3} = 3.4 \times 10^{-4}\,s^{-1}$ by multiplying the time scale with a factor of 2.9/3.4, which allows for direct comparison with the former measurements.

3.2. Measurements Without Photolysis and Data Correction

To test the efficiency of the extraction system and the stability of O_3 during the analytical procedure, measurements without photolysis were carried out with either pure O_3 or mixtures of O_3 and the various bath gases (He, Ar, and CO). The experimental procedure followed exactly the above-described procedure of the photolysis experiments but without illuminating the reactor.

These experiments without photolysis showed a small but significant difference between the amounts of O_3 recovered between the second and third expansion, i.e. $[O_3(\text{start})] < [O_3(\text{end})]$, which implies that some O_3 was lost without photolysis. This loss of 7% for O_3 only and 2–3% for He, Ar, and CO experiments was associated with isotopic changes of 0.1–0.2‰ and 0.1–0.4‰ for $\delta^{17}O$ and $\delta^{18}O$, respectively. We correspondingly subtracted the values of the experiments without photolysis from the measured raw data of the photolysis experiments (see Table S3 in the supporting information).

3.3. Uncertainty Estimates

The results from the photolysis experiments ($\delta^{17}O$, $\delta^{18}O$, and ln(f) of O_3) and the corresponding model results are shown as a function of irradiation time in Figures 3a–3c.

Uncertainties in $\delta^{17}O$ and $\delta^{18}O$ are derived from the stability of mass spectrometric measurements and the sample transfer procedure. They have been determined from repeat experiments and are between 0.1 and 0.5‰ for ^{18}O and 0.1 and 0.3‰ for ^{17}O depending on the experiment and its bath gas. The total error (σ) in $\delta^{17}O$ and $\delta^{18}O$ of the measurements includes the error arising from the correction

value obtained from the experiments without photolysis and is calculated according to the standard rules of error propagation:

$$\sigma = \sqrt{(\sigma_{O_3\text{end}})^2 + (\sigma_{O_3\text{start}})^2 + (\sigma_{\text{darkcorrection}})^2} \quad (14)$$

The uncertainty in ln(f) has been derived from dedicated sampling runs on pure CO_2 gas or on CO_2 admixed to various bath gases. Repeated transfers showed a $>$ 99.5% sampling efficiency for CO_2, which allowed us to use the sampling simulations on CO_2 for establishing the uncertainty budget of the sampling procedure. A slight nonlinearity in the sensor P2 (connected to the reference volume) has been found, and this has been taken into account to measure the pressures of O_3(end) and O_3(start) after (p_a) and before photolysis (p_b) via the blank run. Taking small variations of temperature into account, ln(f) is given by

$$\ln(f) = \ln\left(\frac{p_a/T_a}{p_b/T_b}\right) = \ln\left(\frac{(1+\gamma p_1)p_1 T_b}{\alpha(1+\gamma p_2)p_2 T_a}\right), \quad (15)$$

where $\alpha = 0.694$ (±0.002) is an experimentally defined expansion factor which accounts for the different volumes between reactor and the aliquot for the initial O_3 (blank), $\gamma = 2.2$ (±2.5) mPa^{-1} the nonlinearity coefficient of the pressure sensor, p_1 and p_2 the pressure readings of the sample and the blank, respectively, and T_a and T_b the temperatures when the two readings were made. Pressure readings have relative standard uncertainties $u_r(p)$ of 1.8% each, and the maximum temperature difference $T_a - T_b$ was 1 K, which leads to a relative standard uncertainty of $u_r(T_b/T_a) = 0.001$. The total uncertainty of ln(f) has been calculated from (14) using standard rules of uncertainty propagation from the individual components, γ, α, T, and p. Uncertainties are dominated by the pressure readings and can therefore be considered statistically independent. Values depend slightly on the degree of conversion and are between 2.5 and 2.7% (1σ).

We also have investigated the sensitivity of our derived photolysis induced fractionation values with respect to changes of reaction rates within their uncertainty limits. Generally, we assumed an uncertainty of 10%, except when rates were taken from *Sander et al.* [2011], where 1σ-uncertainty ranges are stated. It was found that uncertainties in the rate coefficient of the $O(^3P) + O_2 + M$ and the $O(^3P) + CO + M$ reactions had a small impact on the result (0.8‰ and 0.6‰, respectively), all others ((R1), (R3), (R5a), (R5b), and (R6)) changed the result by not more than 0.2‰. Altogether, the uncertainty in rate coefficients contributes 1.0 and 0.5‰ to uncertainties in $\varepsilon_{O_3+h\nu}$ of $^{50}O_3$ and $^{49}O_3$, respectively.

While the well-known symmetry dependent fractionation effects in O_3 formation are included in the kinetic model, fractionation effects in O_3 photolysis are based on assuming a statistical distribution of the heavy oxygen in O_3. In an additional sensitivity experiment, it was found that implementing different fractionation values for the symmetric and asymmetric isotopomers (e.g., $\varepsilon_{(OQO)} = 2 \times \varepsilon_{(OOQ)}$) in the model had no significant influence on the final result presented in section 3.

3.4. O_3 Photolysis: Experimental and Kinetic Modeling Results

As $J_{O_3} = 3.4 \times 10^{-4}\,s^{-1}$ was derived from a fit to the O_3 only experiments, the model reproduces ln(f) for these measurements very well. The isotopic composition in the O_3 only experiments shows an increase of $\delta^{17}O$ and $\delta^{18}O$ with time (Figures 3a and 3b). After 30 min, $\delta^{17}O$ reaches about 9‰ and $\delta^{18}O$ increases to 16.5‰. Also, because formation of new O_3 is negligible in these experiments (Figure 2), the observed enrichments are caused by isotope effects in photolysis and chemical removal. The overall fractionation constant $(\varepsilon_{O_3+h\nu} + \varepsilon_{O_3+O})/2$ can be determined from a Rayleigh fractionation plot (Figures 4a and 4b). We find mean values of −14‰ and −7‰ for ^{18}O and ^{17}O, respectively. With these values, the model reproduces the measurements for the O_3 only experiments very well.

In presence of He or Ar bath gas, the apparent O_3 removal rate (Figure 3c) decreases due to the increased importance of O_3 formation (R2) with He or Ar acting as a third body. Due to the large enrichments associated with the formation of this secondary O_3, δ values are higher than in the O_3 only experiments. As the influence of the formation reaction increases with reaction time, the isotope enrichments do not increase linearly in time anymore. In addition, the enrichments are not mass dependent; $\delta^{17}O$ increases to 18‰ and $\delta^{18}O$ to 24‰ after 30 min of photolysis (Figures 3a and 3b). Similar results are obtained for O_3 photolysis in Ar as bath gas, which results in slightly higher enrichments compared to the O_3 + He measurements. This is due to the higher quenching efficiency of Ar that increases the importance of the secondary O_3 formation

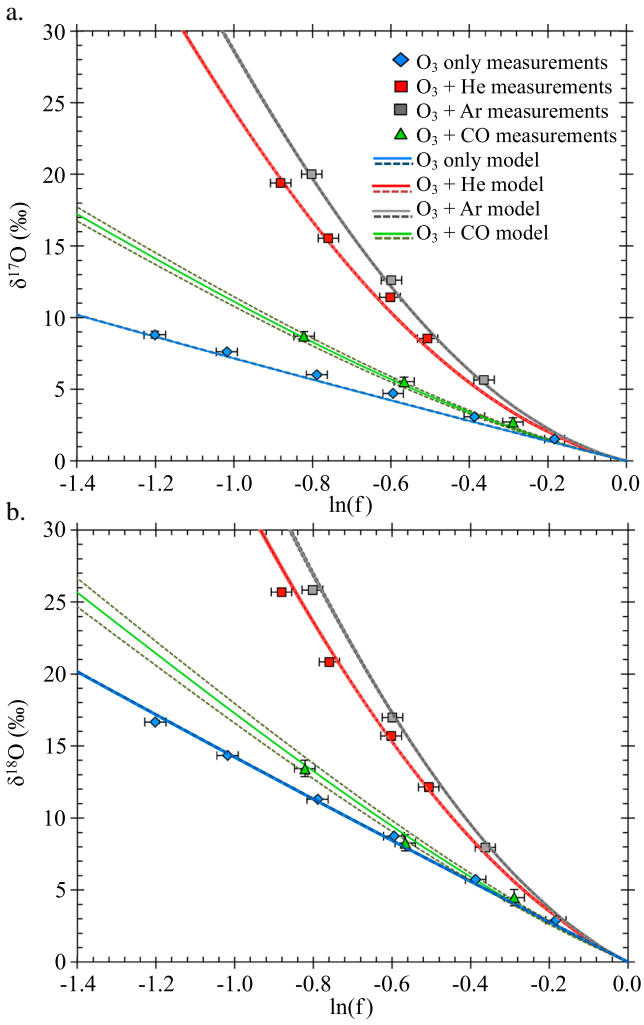

Figure 4. Rayleigh fractionation plots. Symbols represent measurements, and lines represent modeled data. Red: O_3 in He, grey: O_3 in Ar, green: O_3 in CO, and blue: pure O_3 experiments. Solid lines show model output with fractionation in $O_3 + h\nu$ of −16.1 and −8.05‰ for ^{18}O and ^{17}O, respectively. Fractionations in $O_3 + O$ are −11.9 and −5.95‰ for ^{18}O and ^{17}O. Dashed lines define fractionations within our experimental error of $1\sigma \pm 1.4$‰ for $^{18}\varepsilon$ and ±0.7‰ for $^{17}\varepsilon$.

pathway (Figures 3a and 3b). The good agreement between model and experiment suggests that the isotope effects in the O_3 formation reactions have been adequately assigned and that the freshly formed O_3 is responsible for the higher δ values, as expected.

For O_3 photolysis in CO bath gas, our model results for $f(O_3)$ differ significantly from the measurements (Figure 3c). The experimental data show a similar temporal evolution of $f(O_3)$ as the experiments with He or Ar as bath gas. The model, on the other hand, predicts an O_3 removal rate that is much smaller than that for $O_3 + He$. This is also what we expected based on the understanding of the reaction system, since O_3 destruction via $O_3 + O$ is suppressed. When only the O_3 concentrations are evaluated, the results suggest that the $O + CO$ reaction may be barely significant and thus much slower than assumed based on the literature values (see above). However, the isotope results in Figures 3a and 3b clearly indicate that O_3 formation is suppressed by the addition of CO. The isotopic composition attained after a certain time is much lower than that for the $O_3 + He$ experiments; in fact, it is relatively close to the O_3 only experiments. Also, the temporal evolution of the isotope signatures is much more linear again compared to the experiments with He and Ar, implying that the formation reaction is indeed suppressed.

The unexpected additional loss of O_3 indicates that there is a supplementary O_3 loss channel in the experiments that is not included in the kinetic model calculations. In order to reproduce the temporal evolution of ln(f) of O_3 observed in our measurements, we therefore add an additional bimolecular reaction $O_3 + X$ to the model to account for the unidentified O_3 removal of ~20%. Since the additional decomposition of O_3 only appears in presence of CO, we tentatively assign the following reaction with the value of the rate coefficient k_7 resulting from a best fit to our observations

$$O_3 + CO \rightarrow CO_2 + O_2 \qquad k_7 = 6.5\times10^{-24}\,cm^3s^{-1} \qquad (R7)$$

In addition to the rate coefficient, also the isotope effect in (R7) influences the model results and therefore affects the data analysis. To estimate the uncertainty arising from this unknown parameter, we consider three scenarios in which we assume no fractionation for ^{18}O and ^{17}O (S1), collision fractionation factors for the gas phase reaction $CO + O_3$ of 0.9926 and 0.9963 (S2), or fractionation factors of 0.9798 and 0.9897 based on wall collision frequencies of O_3 (S3). For further motivation and detailed description of these scenarios, we refer to section 4.2.

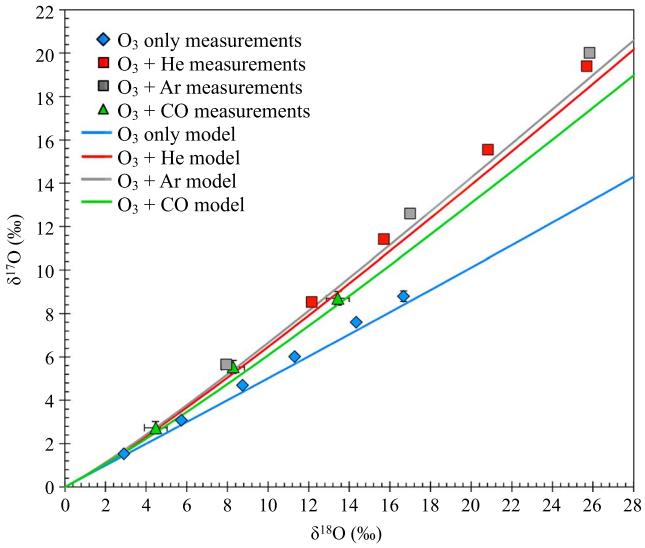

Figure 5. Three-isotope plot. Symbols represent measurements, and solid lines represent model data. Blue: O_3 only, red: O_3 + He, grey: O_3 + Ar, and green: O_3 + CO. Error bars give the total error with 1σ.

3.5. Fractionation in the $O_3 + h\nu$ and $O_3 + O$ Removal Channels

In order to quantify fractionation processes for the different channels $O_3 + h\nu$ and $O_3 + O$, we run the Kintecus model with a range of mass dependent fractionation effects in $O_3 + h\nu$ (R1) and $O_3 + O$ (R3). The sum of both channels is kept fixed to match the results from the O_3 only experiments, $({}^{18}\varepsilon_{O_3+h\nu} + {}^{18}\varepsilon_{O_3+O})/2 = -14‰$ and $({}^{17}\varepsilon_{O_3+h\nu} + {}^{17}\varepsilon_{O_3+O})/2 = -7‰$, but the partitioning between the two channels varies. For example, one combination would be ${}^{18}\varepsilon_{O_3+h\nu} = -8‰$, ${}^{18}\varepsilon_{O_3+O} = -20‰$, and ${}^{17}\varepsilon_{O_3+h\nu} = -4‰$, ${}^{17}\varepsilon_{O_3+O} = -10‰$.

Figures 4a and 4b show the results of the model run including all reactions (R1)–(R7). Assuming no fractionation in the unidentified (R7) (S1), fractionations in $O_3 + h\nu$ and $O_3 + O$ were then adjusted in order to obtain a best fit to our experiments with CO bath gas. Model results that agree with our experimental observations within the errors provide a range of fractionation values for the two individual channels ${}^{18}\varepsilon_{O_3+h\nu}$ and ${}^{18}\varepsilon_{O_3+O}$:

$$ {}^{18}\varepsilon_{O_3+h\nu} = -16.1\ (\pm\ 1.4)‰, {}^{17}\varepsilon_{O_3+h\nu} = -8.05\ (\pm\ 0.7)‰ \text{ and} $$

$$ {}^{18}\varepsilon_{O_3+O} = -11.9\ (\pm\ 1.4)‰, {}^{17}\varepsilon_{O_3+O} = -5.95\ (\pm\ 0.7)‰. $$

Note that uncertainty values reflect measurement, fit, and model errors, the latter comprising uncertainties in rate coefficients, but not differences in scenarios. Assuming strong isotope fractionations of ~20 and ~10‰ for ^{18}O and ^{17}O for (R7) (from scenario S3), the fractionation values in $O_3 + h\nu$ and $O_3 + O$ under our experimental conditions change to

$$ {}^{18}\varepsilon_{O_3+h\nu} = -9.4\ (\pm\ 1.4)‰, {}^{17}\varepsilon_{O_3+h\nu} = -4.7\ (\pm\ 0.7)‰ \text{ and} $$

$$ {}^{18}\varepsilon_{O_3+O} = -18.6\ (\pm\ 1.4)‰, {}^{17}\varepsilon_{O_3+O} = -9.3\ (\pm\ 0.7)‰. $$

The best fit values for ε were obtained using total least squares regression on the sum $\delta^{17}O + \delta^{18}O$ as a function of ln(f) in order to take into account uncertainties in both coordinates (δ and ln(f)). Taking the sum of $\delta^{17}O$ and $\delta^{18}O$ guaranteed that all measurement data were statistically independent. Monte Carlo simulations were employed to verify that our fitting procedure did not introduce a bias in the parameter estimation. Total errors in $\delta^{17}O$ and $\delta^{18}O$ of the $O_3 + CO$ experiments are 0.3‰ and 0.5‰, respectively, leading to an uncertainty of 0.6‰ for the sum signal.

Whereas the fractionation during visible light photolysis is expected to depend on wavelength (see below) and can thus be different for different photolysis lamps, the fractionation in the $O_3 + O$ reaction is independent of the light source and should be a fundamental quantity at the pressure and temperature of the experiment.

3.6. Three-Isotope Plot

Figure 5 illustrates the experimental data in a three-isotope plot. The slopes for the three distinct experiments are different. The data from the O_3 only experiment show a mass-dependent slope (~0.53), in good agreement with the results of *Chakraborty and Bhattacharya* [2003]. As fractionations represent averages of the fractionation constants in O_3 photolysis (R1) and O_3 destruction via $O + O_3$ (R3), we consider it extremely unlikely that the individual reactions follow non-mass dependent fractionation manner and

coincidentally sum up to produce a mass-dependent signature again. This is why the model scenarios in the $O_3 + CO$ experiments presented above were carried out assuming a mass-dependent fractionation in both channels. Experiments in the presence of He or Ar result in clearly mass-independently fractionated O_3 (slope ~ 0.74). The model allows to clearly attributing it to the influence of O_3 formation (R2), because these are the only (necessary) mass-independently fractionating reactions in the model.

In our experiments with CO as bath gas, the three-isotope slope is lower than for the $O_3 + He/Ar$ experiments (slope ~0.62). As shown in Figure 2, under these conditions the O_3 formation reaction (R2) is strongly diminished but still responsible for about 10% of the O removal in the first 30 min of photolysis. The fact that the model fits the experimental results well without any other source of non-mass-dependent fractionation again shows that O_3 formation is most likely the only underlying cause of the observed departure from the mass-dependent three-isotope slope.

4. Discussion

4.1. Additional O_3 Removal in $CO + O_3$ Gas Mixtures

The results from the kinetic model convincingly show that the experimental setup should be adequate to separately quantify fractionation factors for O_3 photolysis and O_3 destruction using the reaction of O atoms with CO as a quencher. However, we observe a clear discrepancy between experimental and model results for $f(O_3)$ in the $O_3 + CO$ experiments.

Analysis of the raw data shows that a significant loss of O_3 occurs immediately after mixing CO and O_3. The O_3 extracted from O_3-CO mixtures (in all expansions) is always ~20% lower than when the same amount of O_3 is extracted either without a bath gas or in He/Ar mixtures. The initial loss of O_3 is attributed to fast and possible catalytic reactions with impurities in the CO reactant. We note that several investigations of the $CO + O_3$ system in the literature have reported similar problems of interfering reactions [*Arin and Warneck*, 1972; *Slanger et al*., 1972]. Adding a carbonyl trap to purify the CO had no effect on the initial loss.

Whereas an initial, fast O_3 loss is undesired, our final results should principally not be affected (as long as the loss is rapid and the gas mixture sufficiently stable afterward) since the amount and isotopic composition of the initial O_3 is determined independently for each single photolysis experiment.

The experiments without photolysis indeed demonstrate that only a much smaller loss of O_3 (2-3%/h) occurs during the period the gas stays in the discharge reactor between the first expansion (used for photolysis) and the third expansion (used to determine O_3(start)). This is faster than what is expected from thermal decomposition ($k_{td} = 1.65 \times 10^{-9}$ exp(−11435 K/T) $cm^3\,s^{-1}$ [M] ~ 0.3%/h, following *Steinfeld et al*. [1987] and *Baulch et al*. [1976]), which must be excluded as viable ozone sink anyway, because no loss is observed using Ar and He as a bath gas. A possible source for this additional loss might be decomposition on the metal tips of the electrodes in the discharge reactor, to which the gas mixtures are exposed up to 4 h during the experiment.

Data are corrected for (a) the initial loss of O_3 occurring at the moment of mixing O_3 and CO and (b) for the loss of O_3 occurring during the measurements without photolysis during the standing time in the discharge reactor; however, an additional loss of O_3 is observed in the $O_3 + CO$ photolysis experiments. The experimental procedure in the $O_3 + CO$ experiments is identical to the $O_3 + He/Ar$ experiments, and numerous tests showed that gas-handling errors could not cause the observed discrepancy. This indicates that an additional O_3 destruction reaction, which accounts for a loss of 20%, is occurring in the experiments employing CO. In principle, such an additional O_3 removal can occur either via loss on the reactor surfaces or via an additional gas phase reaction. An important argument against surface reactions is the fact that the additional loss is not observed for O_3 only experiments and O_3-He/Ar mixtures, but occurs only when CO is used as bath gas. This suggests that additional gas phase reactions may occur in the presence of CO, and one possibility is photochemical recycling of HO_x species, involving catalytic reactions such as

$$CO + OH \rightarrow CO_2 + H \quad k_8 = 1.5\times10^{-13}\,cm^3s^{-1} \tag{R8}$$

$$H + O_3 \rightarrow OH + O_2 \quad k_9 = 2.9\times10^{-11}\,cm^3s^{-1}. \tag{R9}$$

Table 2. Best Fit for Different Model Scenarios (S1–S3)[a]

	ε_{O_3+hv} (‰)		ε_{O_3+O} (‰)		α (O_3 + X)		
	^{18}O	^{17}O	^{18}O	^{17}O	^{18}O	^{17}O	Notes
S1	−16.1 ± 1.4	−8.05 ± 0.7	−11.9 ± 1.4	−5.95 ± 0.7	1	1	O_3 + CO (surface), O_3 + H (gas phase)
S2	−13.4 ± 1.4	−6.7 ±0.7	−14.6 ± 1.4	−7.3 ± 0.7	0.9926	0.9963	O_3 + CO (gas phase) incompatible with previous work
S3	−9.4 ± 1.4	−4.7 ± 0.7	−18.6 ± 1.4	−9.3 ± 0.7	0.9798	0.9897	collisional controlled surface loss of O_3

[a]Errors are obtained as described in section 3.3.

Sources of OH may come from organic contaminations in the original CO, possible outgassing from the epoxy glue upon irradiation, or reaction of excited state O(^{1}D) radicals, generated from possibly remaining UV light that penetrates the filter, with water levels in the reactor.

Simone [2014] showed that when O(^{1}D) radicals are produced from O_3 photolysis, catalytic radical chemistry involving HO_x radicals can strongly affect experiments in photolysis reactors. In order to exclude OH from production of O(^{1}D) via UV photolysis, we performed an experiment where two optical filters (GG455 and GG420) were used in series. The additional loss of O_3 remained the same; and therefore, catalytic reaction cycles initiated by O(^{1}D) can be excluded as source for the extra O_3 removal. The most likely scenario is, therefore, a contribution of gas phase reactions involving unknown, likely organic, contaminations.

Since we were not able to analytically identify the source reaction of the 20% loss of O_3, we included in the kinetic modeling a reaction O_3 + X and assign a range of possible fractionations to this reaction, as discussed in the following section (4.2.) Technically, we implement this reaction in the Kintecus® code as an additional reaction pathway between O_3 and CO (R7). Since CO levels remain virtually constant during an experiment; this results in an additional pseudo first-order reaction for removal of O_3. The implemented rate coefficient for the total reaction (R7) is then higher than upper limits derived from earlier results [*Arin and Warneck*, 1972], but it should be noted that the largest part of this is actually due to the parameterization of the reaction O_3 + X.

4.2. Different Model Scenarios for Additional O_3 Removal

To account for the additional loss of O_3 observed in our experiments, we add an additional O_3 removal reaction (R7) to the kinetic model. Since the source of O_3 loss could not be identified by analytical means, different scenarios needed to be considered to account for the supplemental loss of O_3. In Table 2, we illustrate three scenarios (S1–S3). Depending on the isotope fractionation in the removal process, different fractionation values for the O_3 + hv and O_3 + O reaction channels are derived.

In scenario S1, we assume that O_3 is removed without isotope fractionation ($\alpha = 1$). This scenario may correspond to heterogeneous reaction of O_3 + CO on the reactor wall or the metal tips of the discharge electrodes, or to the catalytic O_3 removal by H (R9) in the gas phase. It has to be noted that surface reactions would occur independent of photolysis, which is not in agreement with our observations, because a correction for the loss of O_3 in experiments without photolysis is already applied to the data. The catalytic pathway may, therefore, be a more realistic hypothesis. Since mass difference between H and O_3 are large, isotope effects related to differences in collisional frequencies are of minor importance. With values of 0.4‰ in ^{18}O and 0.2‰ in ^{17}O, they are rather small and can therefore be neglected. The scenario leads to

$$^{18}\varepsilon_{O_3+hv} = -16.1\ (\pm 1.4)‰ \text{ and } ^{17}\varepsilon_{O_3+hv} = -8.05\ (\pm 0.7)‰ \text{ for photolysis and}$$

$$^{18}\varepsilon_{O_3+O} = -11.9\ (\pm 1.4)‰ \text{ and } ^{17}\varepsilon_{O_3+O} = -5.95\ (\pm 0.7)‰ \text{ for chemical removal,}$$

which corresponds to the highest possible fractionation values, in the photolysis and the lowest possible fractionations in the O + O_3 reaction, as derived by the model calculations.

Scenario S2 uses a calculated isotope effect for direct reaction of O_3 with CO in the gas phase. The corresponding isotope effect is equal to the collisional fractionation factors of about 0.9926 and 0.9963 for ^{18}O and ^{17}O (S2), which are obtained from

$$\alpha_{O_3+CO} = \sqrt{\frac{(m_{O_3} + m_{CO})/(m_{O_3} \times m_{CO})}{(m_{(^{48}O_3)} + m_{CO})/(m_{(^{48}O_3)} \times m_{CO})}} \quad (16)$$

In order to explain the observed rate of O_3 removal, this reaction would have to proceed with a rate coefficient of $k_{O_3+CO} = 6.5 \times 10^{-24}\,cm^3\,s^{-1}$ to explain the observed additional loss of O_3. Although the rate coefficient is low, literature suggests an even lower rate coefficient with an upper limit of $\leq 4 \times 10^{-25}\,cm^3\,s^{-1}$ [*Arin and Warneck*, 1972]. Therefore, this scenario must be ruled out.

In a third scenario (S3), we again consider loss of ozone at the surface, but now assuming that the removal is controlled by the wall collision frequency, leading to fractionation factors as high as $\alpha = 0.9798$ and 0.9897 for ^{18}O and ^{17}O, respectively. We note again that such a process should also happen in the dark and, therefore, be included in the correction value obtained from the measurements without photolysis, but we consider it conceptually to determine the range of possible fractionation values. Such a fractionation in the additional removal would result in fractionation values of

$$^{18}\varepsilon_{O_3+h\nu} = -9.4\ (\pm\ 1.4)‰ \text{ and } ^{17}\varepsilon_{O_3+h\nu} = -4.7\ (\pm\ 0.7)‰ \text{ for photolysis and}$$

$$^{18}\varepsilon_{O_3+O} = -18.6\ (\pm\ 1.4)‰ \text{ and } ^{17}\varepsilon_{O_3+O} = -9.3\ (\pm\ 0.7)‰ \text{ for chemical removal.}$$

These scenarios span the range of fractionation factors for the unidentified removal that we consider realistic under the experimental conditions. Despite thorough investigations, the nature of the additional removal could not be identified. We therefore, advocate the corresponding fractionation values in Table 2. Note that fractionation values in scenarios 2 and 3 are based on the simplistic assumption of hard sphere collisions, completely neglecting isotope effects due to the energetic barrier that controls the speed of the reaction and other dynamic effects. Surface reactions cannot be ruled out completely, even though they are less compatible with our observations. We therefore might use scenario S3 as worst case to determine the uncertainty of our derived fractionation values. Based thereon, we derive lower values for the fractionation constants in the photolysis of about −9 and −4‰ for ^{18}O and ^{17}O. This solidly confirms that the fractionation in the predominant Chappuis band photolysis leads to a slight isotopic enrichment of ozone at about 1 to 2%.

4.3. Isotope Effects in the Visible Light Photolysis of O_3

In this study, we have investigated the isotope effect for O_3 photolysis in the Chappuis band ($500 > \lambda > 700$ nm), which dominates O_3 photolysis in the visible light region. The Chappuis band shows small vibronic structure on both sides of the absorption peak. The observed fractionation in the O_3 only experiments from photolysis and chemical removal together ($\varepsilon_{average} = -14‰$) is very similar to the value of −15‰ that *Chakraborty and Bhattacharya* [2003] found in photolysis experiments using narrowband light sources at 520 (±2) nm and 630 (±4) nm. In all photolysis experiments with pure O_3, photolysis is followed by destruction of another O atom via $O_3 + O$. The comparison with the measurements by *Chakraborty and Bhattacharya* [2003] thus implies that the isotope fractionation in these two narrow wavelength regions is similar to the wavelength integrated photolysis fractionation in our study.

Theoretical calculations based on the measured absorption spectra of $^{16}O^{16}O^{16}O$ and $^{18}O^{18}O^{18}O$ postulated a strong wavelength dependency of the fractionation values in the Chappuis band, however. Based on calculations by *Liang et al.* [2006], fractionations can vary from −107‰ to +25‰ at individual wavelengths for $^{16}O^{16}O^{18}O$ and from −92‰ to +22‰ for $^{16}O^{16}O^{17}O$. Since we are using a broadband light source, the isotope fractionation due to the vibronic structure should largely average out. When the calculated fractionation factors from *Liang et al.* [2006] are folded with the actinic flux spectrum of our photolysis lamp, we calculate slightly negative fractionations for visible light photolysis of symmetric and asymmetric O_3. For $^{16}O^{16}O^{17}O$ and $^{16}O^{16}O^{18}O$, fractionations are −3‰ and −6‰, for $^{16}O^{17}O^{16}O$ and $^{16}O^{18}O^{16}O$, fractionations are −5‰ and −10‰, respectively (see supporting information Figure S2). The absolute discrepancy between our measurements and the theoretical calculations by *Liang et al.* [2006] is about 10‰ or more for $^{18}\varepsilon$. It is likely that this discrepancy is due to the simple ZPE model, as it has been shown to suffer from several shortcomings in predicting fractionation effects in complex molecules as compared to more elaborate models [*Schmidt et al.*, 2013]. While *Schmidt et al.* [2013] found a factor of 3 difference between their full wave packet calculations and the simple ZPE model in the UV photolysis of carbon dioxide, *Ndengue et al.* [2014] also obtained smaller fractionation factors for ozone photolysis compared to the results from *Liang et al.* [2006], as indicated by the prediction of larger atmospheric enrichments.

Cole and Boering [2006] analyzed the data from *Chakraborty and Bhattacharya* [2003] in more detail by applying kinetic modeling, similar to the model used in our study. Importantly, they also implemented fractionation effects in photolysis and $O_3 + O$ separately. In the absence of information on the fractionation in the chemical removal, they used the calculated fractionation for photolysis at the relevant wavelengths from *Liang et al*. [2004] and adjusted the fractionation in the $O + O_3$ reaction in order to fit the results, basically following our equation (10). Their base scenario uses a strong negative fractionation in O_3 photolysis at 520 nm of ${}^{18}\varepsilon_{O_3+hv} = -24‰$ and ${}^{17}\varepsilon_{O_3+hv} = -12.5‰$ from *Liang et al*. [2004]. In order to fit the observed isotopic composition from the experiments (${}^{18}\varepsilon_{obs} = -15‰$), they needed to postulate a negative fractionation in $O_3 + O$ of ${}^{18}\varepsilon_{O_3+O_3} = -60‰$. As the fractionation in the chemical removal has to be the same when O_3 is photolyzed at a different wavelength but the calculated fractionation in photolysis at 630 nm is very different (${}^{18}\varepsilon_{O_3+hv} = +4.2‰$ and ${}^{17}\varepsilon_{O_3+hv} = +2.1‰$), it was not possible to fit the very similar experimental results at both wavelengths with these assumptions.

The results from our experiments imply that the fractionation in the chemical removal is much smaller than what had to be assumed by *Cole and Boering* [2006], which means that the assigned fractionation in visible photolysis (at 520 and 630 nm) from *Liang et al*. [2006] in their study was inadequate. *Cole and Boering* [2006] already discussed that in view of the strong vibronic structure of the O_3 absorption cross section in the Chappuis band, it would be desirable to calculate the fractionation at much higher spectral resolution in order to compare with narrow band light sources and this can indeed lead to large errors.

It is surprising that although the semiempirical calculations predict a large wavelength dependency of the fractionation for photolysis in the Chappuis band [*Miller et al*., 2005; *Liang et al*., 2006], measurements at two different wavelengths from *Chakraborty and Bhattacharya* [2003] and our new broadband results yield very similar fractionation constants for visible light photolysis. It would be interesting to investigate experimentally whether this is a coincidence or whether the wavelength dependence is actually smaller than expected from the semiempirical model calculations.

We note that *Morton et al*. [1990] briefly report on a set of photolysis experiments with visible light around the maximum of the Chappuis band at 590 nm. After 80% of dissociation the isotopic composition was within the experimental uncertainty of 6‰ equal to the initial O_3, and the authors state that any additional isotope effect for $O_3 + O$ or $O_3 + hv$ in the visible light spectrum can be excluded. However, also in these experiments the isotope effect in the chemical removal must have been active, and this would imply that in their experimental setup the photolysis fractionation was actually negative in order to cancel out the enrichment expected from the chemical removal.

Furthermore, additional fractionations can occur in the dominating reaction $CO + O + M$ (R4), but this reaction does not directly involve O_3, whereas (R2) and (R3) do. Nevertheless, (R4) can still affect O_3, but only via an effect on the O atom reservoir, which can then be transferred to O_3 again in the O_3 formation reaction (R2). *Pandey and Bhattacharya* [2006a, 2006b] reported a strong mass-independent fractionation in the reaction $CO + O + M$, but *Simone* [2014] showed that the reported enrichments are likely due to interferences from O_3 formation. Therefore, in our model, we apply no fractionation effects for the CO_2 formation reaction.

4.4. Applications in the Atmosphere

In the atmosphere, O_3 is generally considered to be in photostationary equilibrium between formation and photolysis. The isotopic composition in equilibrium between O_3 formation and O_3 photolysis is the sum of the fractionations in those two processes. The effect of ${}^{18}\varepsilon = -9$ to $-16‰$ in O_3 photolysis, reported in this study, is small but still significant compared to the observed enrichments in $\delta^{18}O$ of ~ 90‰ in the troposphere [*Krankowsky et al*., 1995; *Johnston and Thiemens*, 1997]. Despite the actinic flux spectrum of our light source used for photolysis being different from the actinic flux spectrum in the atmosphere, we expect that these values are somewhat representative for atmospheric ozone dissociation in the Chappuis band. This is due to the fact that we have essentially probed the peak region of that band, and that our pure O_3 results are very similar to the relative short band measurements at 520 and 630 nm of *Chakraborty and Bhattacharya* [2003], which implies that isotope effects from ozone photolysis integrated over several nm in this wavelength region yield somewhat consistent values of about 1 to 2%.

In the middle atmosphere, the odd oxygen sink reaction $O + O_3$ is slow compared to photolysis; and therefore, the associated fractionation will likely be of minor importance for the isotopic composition of O_3 in this region. At the higher altitudes of the lower thermosphere (>105 km), however, the odd oxygen sink reaction becomes a competitive removal channel for ozone [*Allen et al*., 1984]. It will, therefore, well affect the ozone isotopic composition.

5. Conclusions and Outlook

An attempt to separately measure fractionation effects in O_3 photolysis in the Chappuis band and the $O_3 + O$ reaction has been presented. By adding CO as bath gas, we were able to effectively suppress the reaction pathway $O + O_3$ and, therefore, quantify isotope effects in visible light photolysis. Experiments with pure O_3 and O_3 in He or Ar as bath gas could successfully be reproduced with a kinetic model. However, in the presence of CO as bath gas, an additional unidentified removal channel of O_3 leads to a systematic uncertainty. Under consideration of an additional O_3 removal reaction $O_3 + CO$ (R7) with different fractionation values, represented in scenarios S1–S3, we can quantify fractionations in O_3 photolysis and O_3 removal ($O_3 + O$) to range between

$$^{18}\varepsilon_{O_3+hv} = -16.1\ (\pm\ 1.4)‰,\ ^{17}\varepsilon_{O_3+hv} = -8.05\ (\pm\ 0.7)‰$$

$$^{18}\varepsilon_{O_3+O} = -11.9\ (\pm\ 1.4)‰,\ \ ^{17}\varepsilon_{O_3+O} = -4.7\ (\pm\ 0.7)‰\ \text{and}$$

$$^{18}\varepsilon_{O_3+hv} = -9.4\ (\pm\ 1.4)‰,\ \ ^{17}\varepsilon_{O_3+hv} = -4.7\ (\pm\ 0.7)‰$$

$$^{18}\varepsilon_{O_3+O} = -18.6\ (\pm\ 1.4)‰,\ \ ^{17}\varepsilon_{O_3+\ O} = -9.3\ (\pm\ 0.7)‰.$$

With our findings, we could quantify isotope effects in the O_3 photolysis in the Chappuis band and in the $O + O_3$ odd oxygen sink reaction, which provides valuable information for understanding isotope effects affecting ozone isotopic composition in the laboratory. These data also provide an important contribution to the modeling of atmospheric oxygen isotopes. Future photolysis studies employing the CO quencher technique should concentrate on a reduction of side reactions to further constrain individual fractionation factors.

For better understanding of the observed isotopic composition of stratospheric O_3, it would be of considerable interest to study the isotope effects due to O_3 photolysis in the UV spectrum. Furthermore, the determination of wavelength dependent fractionations and isotopologue-specific spectral absorption cross sections of O_3 would provide an important contribution to the understanding of atmospheric O_3 and its isotopic composition.

Acknowledgments
This work was funded by the Marie Curie Initial Training Network INTRAMIF (Initial Training Network in Mass Independent Fractionation) as part of the European Community's Seventh Framework Program (FP7/2007-2013), grant 237890. We thank three anonymous reviewers for their insightful comments. Data for this paper can be requested from Marion Früchtl (Email: m.fruechtl@uu.nl).

References

Allen, M., J. I. Lunine, and Y. L. Yung (1984), The vertical distribution of ozone in the mesosphere and lower thermosphere, *J. Geophys. Res.*, *89*, 4841–4872, doi:10.1029/JD089iD03p04841.

Anderson, S. M., D. Hülsebusch, and K. Mauersberger (1997), Surprising rate coefficients for four isotopic variants of $O+O_2+M$, *J. Chem. Phys.*, *107*(14), 5385, doi:10.1063/1.474247.

Arin, L. M., and P. Warneck (1972), Reaction of ozone with carbon monoxide, *J. Phys. Chem.*, *76*(11), 1514–1516.

Babikov, D., B. K. Kendrick, R. B. Walker, R. T. Pack, P. Fleurat-Lesard, and R. Schinke (2003), Formation of ozone: Metastable states and anomalous isotope effect, *J. Chem. Phys.*, *119*(5), 2577, doi:10.1063/1.1587113.

Baulch, D. L., D. D. Drysdale, J. Duxbury, and S. J. Grant (1976), Homogeneous gas phase reactions of the O_2-O_3 systems, the CO-O_2-H_2 system, and of sulphur-containing species, in *Volume 3 of Evaluated Kinetic Data for High Temperature Reactions*, vol. 118, Butterworth, London.

Brenninkmeijer, C. A. M., C. Janssen, J. Kaiser, T. Röckmann, T. S. Rhee, and S. S. Assonov (2003), Isotope effects in the chemistry of atmospheric trace compounds, *Chem. Rev.*, *103*(12), 5125–62, doi:10.1021/cr020644k.

Chakraborty, S., and S. K. Bhattacharya (2003), Oxygen isotopic fractionation during UV and visible light photodissociation of ozone, *J. Chem. Phys.*, *118*(5), 2164, doi:10.1063/1.1533080.

Cole, A. S., and K. A. Boering (2006), Mass-dependent and non-mass-dependent isotope effects in ozone photolysis: Resolving theory and experiments, *J. Chem. Phys.*, *125*(18), 18,4301–1–18,4301–14, doi:10.1063/1.2363984.

DeMore, W. B. (1972), Pressure dependence and mechanism of the reaction of atomic oxygen and carbon monoxide, *J. Phys. Chem.*, *76*(24), 3527–3532.

Fischer, J., R. R. Gamache, A. Goldman, L. S. Rothman, and A. Perrin (2003), Total internal partition sums for molecular species in the 2000 edition of the HITRAN database, *J. Quant. Spectros. Radiat. Transfer*, *82*(1–4), 401–412, doi:10.1016/S0022-4073(03)00166-3.

Fleurat-Lessard, P., S. Y. Grebenshchikov, R. Schinke, C. Janssen, and D. Krankowsky (2003), Isotope dependence of the $O+O_2$ exchange reaction: Experiment and theory, *J. Chem. Phys.*, *119*(9), 4700–4712, doi:10.1063/1.1595091.

Gao, Y. Q., and R. A. Marcus (2001), Strange and unconventional isotope effects in ozone formation, *Science*, *293*(5528), 259–263, doi:10.1126/science.1058528.

Gao, Y. Q., and R. A. Marcus (2002), On the theory of the strange and unconventional isotopic effects in ozone formation, *J. Chem. Phys.*, *116*(1), 137–154, doi:10.1063/1.1415448.

Haverd, V., G. C. Toon, and D. W. T. Griffith (2005), Evidence for altitude-dependent photolysis-induced ^{18}O isotopic fractionation in stratospheric ozone, *Geophys. Res. Lett.*, *32*, L22808, doi:10.1029/2005GL024049.

Heidenreich, J. E. I., and M. H. Thiemens (1983), A non-mass-dependent isotope effect in the production of ozone from molecular oxygen, *J. Chem. Phys.*, *78*(2), 892–895, doi:10.1063/1.444791.

Hippler, H., R. Rahn, and J. Troe (1990), Temperature and pressure dependence of ozone formation rates in the range 1–1000 bar and 90–370 K, *J. Chem. Phys.*, *93*(9), 6560–6569, doi:10.1063/1.458972.

Ianni, J. C. (2003), A comparison of the Bader-Deuflhard and the Cash-Karp Runge–Kutta integrators for the GRI-MECH 3.0 model based on the chemical kinetics code Kintecus, in *Computational Fluid and Solid Mechanics 2003*, edited by K. J. Bathe, pp. 1368–1372, Elsevier, Oxford, U. K.

Jacob, D. J. (1999), *Introduction to Atmospheric Chemistry*, 267 p., Princeton Univ. Press.

Jaffe, S., and F. S. Klein (1966), Isotopic exchange reactions of atomic oxygen produced by the photolysis of NO_2 at 3660 A*, *Trans. Faraday Soc.*, *62*, 3135–3141.

Janssen, C., and B. Tuzson (2010), Isotope evidence for ozone formation on surfaces, *J. Phys. Chem.*, *114*(36), 9709–19, doi:10.1021/jp1017899.

Janssen, C., J. Guenther, D. Krankowsky, and K. Mauersberger (1999), Relative formation rates of $^{50}O_3$ and $^{52}O_3$ in ^{16}O–^{18}O mixtures, *J. Chem. Phys.*, *111*(16), 7179–7182, doi:10.1063/1.480045.

Janssen, C., J. Guenther, K. Mauersberger, and D. Krankowsy (2001), Kinetic origin of the ozone isotope effect: A critical analysis of enrichments and rate coefficients, *Phys. Chem. Chem. Phys.*, *3*, 4718–4721.

Janssen, C., J. Guenther, D. Krankowsky, and K. Mauersberger (2003), Temperature dependence of ozone rate coefficients and isotopologue fractionation in ^{16}O–^{18}O oxygen mixtures, *Chem. Phys. Lett.*, *367*, 34–38, doi:10.1016/S0009-2614(02)01665-2.

Johnson, D. G., K. W. Jucks, W. A. Traub, and K. V. Chance (2000), Isotopic composition of stratospheric ozone, *J. Geophys. Res.*, *105*(D7), 9025–9031, doi:10.1029/1999JD901167.

Johnston, J. C., and M. H. Thiemens (1997), The isotopic composition of tropospheric ozone in three environments, *J. Geophys. Res.*, *102*(D21), 25,395, doi:10.1029/97JD02075.

Krankowsky, D., F. Bartecki, G. G. Klees, K. Mauersberger, and K. Schellenbach (1995), Measurement of heavy isotope enrichment in tropospheric ozone, *Geophys. Res. Lett.*, *22*(13), 1713–1716, doi:10.1029/95GL01436.

Krankowsky, D., P. Lämmerzahl, K. Mauersberger, C. Janssen, B. Tuzson, and T. Röckmann (2007), Stratospheric ozone isotope fractionations derived from collected samples, *J. Geophys. Res.*, *112*, D08301, doi:10.1029/2006JD007855.

Liang, M.-C., G. A. Blake, and Y. L. Yung (2004), A semianalytic model for photo-induced isotopic fractionation in simple molecules, *J. Geophys. Res.*, *109*, D10308, doi:10.1029/2004JD004539.

Liang, M.-C., F. W. Irion, J. D. Weibel, C. E. Miller, G. A. Blake, and Y. L. Yung (2006), Isotopic composition of stratospheric ozone, *J. Geophys. Res.*, *111*, D02302, doi:10.1029/2005JD006342.

Maeburn, G. M., D. Perner, J. LeCalvé, and M. Bourène (1968), A pulsed-radiolysis study of atomic oxygen reactions in the gas phase, *J. Phys. Chem.*, *107*(4), 3920–3925.

Mauersberger, K. (1981), Measurement of heavy ozone in the stratosphere, *Geophys. Res. Lett.*, *8*(8), 935–937, doi:10.1029/GL008i008p00935.

Mauersberger, K., J. Morton, B. Schueler, and J. Stehr (1993), Multi-isotope study of ozone: Implications for the heavy ozone anomaly, *Geophys. Res. Lett.*, *20*(11), 1031–1034, doi:10.1029/93GL01080.

Mauersberger, K., B. Erbacer, D. Krankowsky, J. Günther, and R. Nickel (1999), Ozone isotope enrichment: Isotopomer-specific rate coefficients, *Science*, *283*(5400), 370–372, doi:10.1126/science.283.5400.370.

Mauersberger, K., P. Lämmerzahl, and D. Krankowsky (2001), Stratospheric ozone isotope enrichments-revisited, *Geophys. Res. Lett.*, *28*(16), 3155–3158, doi:10.1029/2001GL013439.

Mauersberger, K., D. Krankowsky, and C. Janssen (2002), Oxygen isotope processes and transfer reactions, *Space Sci. Rev.*, *106*, 265–279, doi:10.1023/A:1024650007258.

Miller, C. E., R. M. Onorato, M.-C. Liang, and Y. L. Yung (2005), Extraordinary isotopic fractionation in ozone photolysis, *Geophys. Res. Lett.*, *32*, L14814, doi:10.1029/2005GL023160.

Morton, J., J. Barnes, B. Schueler, and K. Mauersberger (1990), Laboratory studies of heavy ozone, *J. Geophys. Res.*, *95*(D1), 901–907, doi:10.1029/JD095iD01p00901.

Ndengue, S., S. Madronich, F. Gatti, H.-D. Meyer, O. Motapon, and R. Jost (2014), Ozone photolysis: Strong isotopologue/isotopomer selectivity in the stratosphere, *J. Geophys. Res. Atmos.*, *119*, 4286–4302, doi:10.1002/2013JD020033.

Pandey, A., and S. K. Bhattacharya (2006a), Anomalous oxygen isotope enrichment in CO_2 produced from O+CO: Estimates based on experimental results and model predictions, *J. Chem. Phys.*, *124*(23), 234301(1–13), doi:10.1063/1.2206584.

Pandey, A., and S. K. Bhattacharya (2006b), Erratum: "Anomalous oxygen isotope enrichment in CO_2 produced from O+CO: Estimates based on experimental results and model predictions, *J. Chem. Phys.*, *124*, 234301, doi:10.1063/1.2345360.

Richet, P., Y. Bottinga, and M. Javoy (1977), A review of hydrogen, carbon, nitrogen, oxygen, sulphur, and chlorine stable isotope fractionation among gaseous molecules, *Ann. Rev. Earth Planet. Sci.*, *5*(196), 65–110.

Rothman, L. S., et al. (2013), The HITRAN2012 molecular spectroscopic database, *J. Quant. Spectros. Radiat. Transfer*, *130*, 4–50, doi:10.1016/j.jqsrt.2013.07.002.

Sander, S. P., et al. (2011), *Chemical Kinetics and Photochemical Data for Use in Atmospheric Studies Evaluation Number 17 NASA Panel for Data Evaluation*, National Aeronautics and Space Administration, Pasadena.

Schmidt, J. A., M. S. Johnson, and R. Schinke (2013), Carbon dioxide photolysis from 150 to 210 nm: Singlet and triplet channel dynamics, UV-spectrum, and isotope effects, *Proc. Natl. Acad. Sci. U.S.A.*, *110*(44), 17,691–17,696, doi:10.1073/pnas.1213083110.

Simonaitis, R., and J. Heicklen (1972), Kinetics and mechanism of the reaction of $O(^3P)$ with carbon monoxide, *J. Chem. Phys.*, *56*(5), 2004–2011, doi:10.1063/1.1677490.

Simone, D. (2014), The production and characterisation of high purity ozone and experimental and modelling studies of anomalous oxygen isotope effects in the formation of carbon dioxide from irradiated mixtures of carbon monoxide and ozone or oxygen, 1–146 pp., PhD thesis L'Université Pierre et Marie Currie.

Slanger, T., B. J. Wood, and G. Black (1972), Kinetics of $O(^3P)$ + CO+M recombination, *J. Chem. Phys.*, *57*(1), 233–238.

Steinfeld, J. M., S. M. Adler-Golden, and J. W. Gallagher (1987), Critical survey of data on the spectroscopy and kinetics of ozone in the mesosphere and thermosphere, *J. Phys. Chem. Ref. Data*, *16*(4), 911–951, doi:10.1063/1.555796.

Stuhl, F., and H. Niki (1971), Measurements of rate constants for termolecular reactions of $O(^3P)$ with NO, O_2, CO, N_2, and CO_2 using a pulsed vacuum-UV photolysis chemiluminescent method, *J. Chem. Phys.*, *55*(8), 3943–3953, doi:10.1063/1.1676682.

Urey, H. C. (1947), The thermodynamic properties of isotopic substances, *J. Chem. Soc.*, 562–581.

Wiegel, A. A., A. S. Cole, K. J. Hoag, E. L. Atlas, S. M. Schauffler, and K. A. Boering (2013), Unexpected variations in the triple oxygen isotope composition of stratospheric carbon dioxide, *Proc. Natl. Acad. Sci. U.S.A.*, *110*(44), 17,680–5, doi:10.1073/pnas.1213082110.